

Characterization of low-pressure arc plasma in large volumes

S Avtaeva², V Gorokhovskiy¹, S Myers¹, A Obrusnik³, S Robertson⁴, E Shunko⁵,
Z Zembower¹

¹Vapor Technologies, Inc., Longmont, Colorado, USA

²Institute of Laser Physics, Novosibirsk, Russia

³Plasma Solve, Ltd., Brno, Czechia

⁴University of Colorado, Boulder, Colorado, USA

⁵AMPRES, Inc., Ypsilanti, Michigan, USA

E-mail: vgorokhovskiy@vaportech.com

Abstract. Study of the large area low-pressure arc discharge plasma in Ar and Ar-N₂ mixtures is presented. The low-pressure arc discharge in large chambers was ignited between planar vacuum arc cathode with magnetic steering of arc spots and surrounding grounded primary anode while long-length remote arc discharge is extended toward remote linear anode parallel to the cathode plate. The arc column was moving up and down perpendicular to the cathode-to-remote anode direction, following the movement of the cathodic arc spots. *I-V* characteristics of the remote arc discharge were studied by electrophysical measurements. Electron density, electron temperature, and dissociation of nitrogen molecules in the low-pressure DC arc discharge in pure argon and Ar-N₂ mixtures at pressures ranging 1-20 mTorr were studied by electrostatic probes, MW resonant probe, ion energy analyzer and spectral methods at various remote anode currents and gas composition.

1. Introduction

Nowadays large area plasma of low-pressure discharges is utilized to increase productivity of plasma processes such as surface treatment, dielectric and semiconductor etching and thin film deposition [1, 2]. The low-pressure arc is a powerful source of dense plasma which can be used in various technologies such as surface engineering processes [3], electric propulsion [4], and isotope separation [5]. The low-pressure (LP) arc as well as vacuum arc were intensively studied from 1950 and have been understood well enough [6-9]. To develop the large area LP arc discharge we use a remote anode together with the primary anode. The remote anode draws out electrons from a primary discharge and forces them to move for a long distance producing large-area plasma. The properties of the large area LP arc discharge plasma are different from conventional vacuum arc discharges and are less investigated and understood. The paper holds results of versatile studying parameters of the LP arc discharge in Ar and Ar-N₂ mixtures.

2. Experimental setup and diagnostic methods

The experimental setup is shown in figure 1. Experiments were conducted in the horizontal rectangular

discharge chamber of $2 \times 1 \times 0.25 \text{ m}^3$. The primary arc (PA) discharge was ignited between planar stainless cathode separated from the discharge chamber by chevron baffle served together with chamber walls as primary anode. The cathodic vacuum arc spots move along the periphery of the vertically positioned cathode target's evaporation side up and down by magnetic steering system utilizing a set of permanent magnets positioned behind the cathode target plate (the target length was 1m). The remote arc (RA) discharge, powered by RA power supply utilizing two Miller XMT 456 connected in series with 180V OCV, was extended horizontally beyond the chevron baffle, positioned immediately after the cathode, along the discharge chamber between the cathode and the main remote anode, making the length of RA column approximately 1.5 m. The resistances both in the primary arc circuit R1 and in the remote arc circuit R2 were approximately 0.5 Ohm each. The additional intermediate remote anode was installed at about mid-point location between the cathode and the main remote anode. The intermediate anode was connected to the positive terminal of the RA discharge power supply via variable resistor R3.

All experiments were conducted at primary arc current of 75 A while the remote anode current was varied from 5 to 200 A. Gas pressure was changed from 2 to 25 mTorr. Ar-N₂ mixture composition was changed from pure argon up to pure nitrogen. The RA discharge is spatially uniform in lateral direction while in a direction perpendicular to the cathode-remote anode axes the well-forming RA column was observed, which was moving up and down dragged by the movement of the cathodic arc spots. A set of multi-channel ion-collecting probes were placed vertically to estimate the dynamic of RA plasma column vertical movement. Each of the ion collecting probes was made of stainless steel (SS) disk, 5 mm in diameter positioned perpendicular to the remote arc column axes and charged negatively to -20V in reference to the floating shield. Langmuir and hairpin probes were placed at the discharge axis as it is shown in figure 1 with ability of lateral positioning in a direction perpendicular to the cathode-remote anode axis.

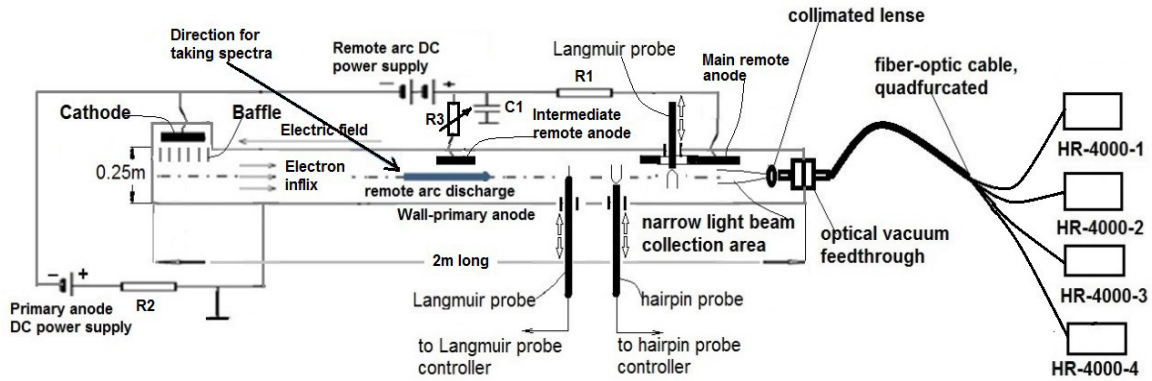


Figure 1. The low-pressure arc discharge setup in long chamber: planar view.

Both the cylindrical Langmuir probe and the hairpin probe were manufactured by Hiden Analytics. Langmuir probe used tungsten wire filament 150 μm in diameter with active length of 10 mm, which was enclosed in an alumina tube. Details on the T_e and n_e measurements using the Langmuir probe technique in the discharge plasma are described elsewhere [10]. The principle of measuring electron density by the hairpin probe is based on the relative shift of its resonance frequency from the resonance frequency in vacuum [11]. The ion energies distribution in RA discharge column were measured by the gridded energy analyzer (GEA) probe, which was immersed within the RA discharge plasma with ability both for lateral positioning and rotation, which allowed to position its front orifice either facing the cathode or the remote anode. Five grids and ion collector are employed in the GEA. The ion energy distribution function $f(V)$

was extracted by differentiation of the collector ion current $I_c(V_a)$ over the voltage applied to the analyzing grid V_a [12].

In addition, electron temperature T_e and density n_e were measured using optical emission spectroscopy (OES) technique. The T_e was measured by the intensity-ratio of two ArI lines 415.86 and 306.65 nm, which is a function of the T_e at conditions of the corona equilibrium. In Ar-N₂ RA discharge the T_e was also estimated using an intensity ratio of the (0-0) vibrational band of the N₂ 1st negative system (391.4 nm) and (0-0) vibrational band of the N₂ 2nd positive system (337.1 nm) [10]. The n_e in the argon RA discharge was obtained using the intensity ratio I_i/I_a of ArII 487.98 nm and ArI 451.07 nm lines [10]. In Ar-N₂ RA discharge we also estimated n_e using contour graph of N₂($C^3\Pi_u, \nu=1$)/ N₂($C^3\Pi_u, \nu=0$) population ratios [13]. Monitoring the nitrogen dissociation degree was carried out using $I_{\text{NI},868.03}/I_{\text{ArI},852.14}$ and $I_{\text{NI},862.92}/I_{\text{ArI},852.14}$ intensity ratios [10]. Four HR-4000 Ocean Optics spectrometers with full bandwidths of 199-972 nm having optical resolutions of ~ 0.03 nm (with gratings of 1200 L/mm) and high sensitivity detectors were utilized to measure intensities of the spectral lines. Light is gathered along the area of length ~ 2 m. A collimated long-focus lens collected light along very narrow area near to center of the chamber and focused it at the fiber optic cable divided in 4 channels connected with entrance slits of the spectrometers. The relative sensitivity of the devices depending on wavelength was calibrated using the DH-2000-CAL.

3. Experimental results and discussion

The I - V characteristic of the remote arc discharge in argon is shown in figure 2a. The V - P characteristics of remote and intermediate anodes are shown in figure 2b,c. It can be seen that RA voltage U_{RA} increases with increase of RA current I_{RA} from 20A to ~ 60 A and saturates at $I_{RA} > 60$ A. U_{RA} decreases when discharge pressure increases, which can be also seen from V - P characteristics of the intermediate anode in different gas mixtures, which also show that adding nitrogen to argon lead to increase of the RA voltage drop.

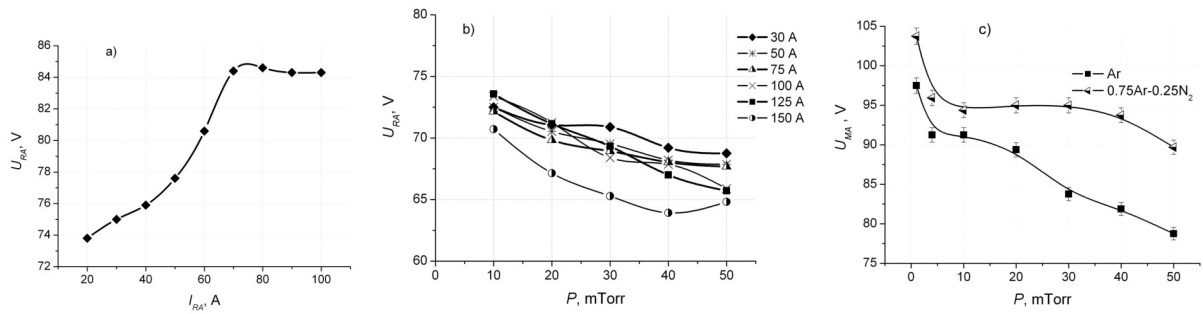


Figure 2. I - V characteristics of RA discharge in argon at 2.5 mTorr (a); the remote anode voltage in Ar versus pressure at different remote arc currents (b) and intermediate anode voltage versus pressure at remote arc current 20A (c).

Typical set of signals from four disk ion collectors (probes) located at different heights from the bottom to the top levels aligned with the primary cathode target is shown in figure 3, demonstrating spikes of the ion currents collected by each disk-probe when the remote arc column is crossing the probe during its vertical movement.

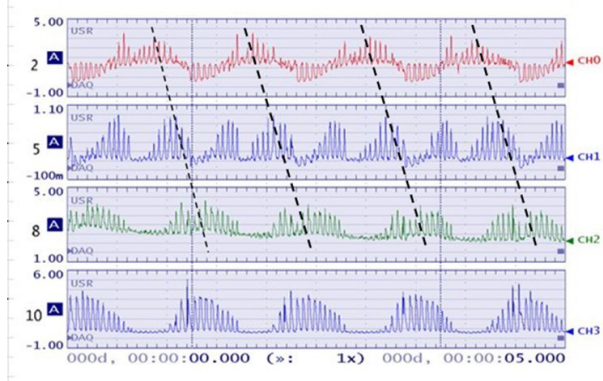


Figure 3. Multi-probe ion current signals collected simultaneously from 4 disk-probes, located at different vertical positions parallel to the tubular cathode target axes at -20V applied to active probes relative to surrounding metal shields. The primary arc current I_{PA} is 150A and the remote anode current I_{RA} is 100A . The dashed lines are indicating the shift in time between the collecting signals of the disk-probes located at different heights one after another.

It should be noted that usually there are more than one traveling arc spots on SS cathode target at the current exceeding 50A , which is minimum arc current per one spot for stainless steel. This can explain that some of the disk-probes can show the signal outside of the time-shifting line. It was found that the arc spot speed increases with increase of the RA current and the corresponding increase of the total arc current, resulting in increase of the arc steering magnetic field in agreement with the vacuum arc retrograde movement law [9]. One can see that each signal representing arc column crossing the probe is split in number of higher frequency fringes. This can be attributed to helical movement of the arc spot steered by longitudinal magnetic field which periodically moves the arc spots to the side of the target cylinder opposite to the side facing the remote anode hence increasing the remote arc plasma impedance and decreasing the plasma density within the remote arc column. The estimated speed of vertical movement of arc spots is ranging from 5 to 10 m/s which is typical for the arc current of $\sim 100\text{A}$ [9].

The IEDFs obtained with GEA in argon RA plasma are shown in figure 4. It can be seen that in RA plasma there are two well-defined groups of ions, one consisting of ions having mean energy of \sim several eV and another group with most probable ion energy $\sim 20\text{eV}$ and FWHM $\sim 10\text{-}15\text{ eV}$.

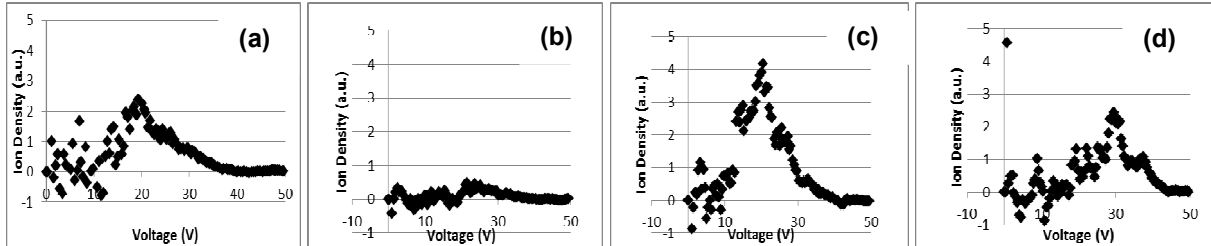


Figure 4. IEDF of RA plasma in argon at $P=2\text{ mTorr}$, (a) $I_{RA}=100\text{A}$, GEA facing cathode; (b) $I_{RA}=100\text{A}$, GEA facing anode; (c) $I_{RA}=300\text{A}$, GEA facing cathode; (d) $I_{RA}=300\text{A}$, GEA facing anode.

At $I_{RA}=300\text{A}$ and GEA facing anode the maximum ion density of high-energy ion group is observed at 30 eV . The increase of ion energies taken from the anode side versus energies of ions incoming from the cathode side can be explained by momentum and energy transfer from current carried electrons to ions in a high current RA discharge. It can also be seen that ion density increases with increase of remote anode current.

The plasma potential measured with Langmuir probe by max slope and by a derivative of the $I-V$ probe characteristics amounts to $16\text{-}20\text{ V}$ and depends weak on RA current. T_e decreases a little with RA current I_{RA} and with gas pressure P and lies in range of $1.8\text{-}3.0\text{ eV}$. The T_e dependences on I_{RA} and P measured with Langmuir probe are like that obtained using the intensity ratio but T_e values measured with the probe are higher on about 0.5 eV as compared with obtained using the intensity ratio.

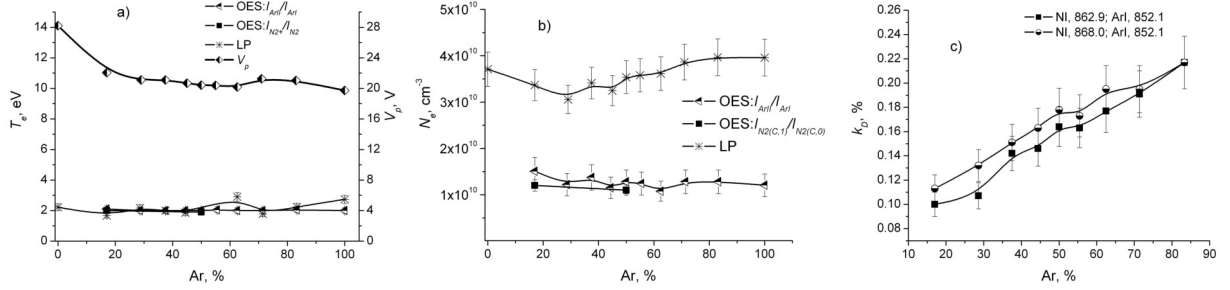


Figure 5. T_e , V_p (a) and n_e (b) obtained with OES and with Langmuir probe, as well as N₂ dissociation degree (c) in the arc discharge as functions of the Ar fraction in Ar-N₂ mixtures; $P=2.5$ mTorr, $I_{PA}=I_{RA}=75$ A.

The electron density in the low-pressure arc grows both with RA current and with gas pressure. In Ar-N₂ arc discharges both $I_{ArII,487}/I_{ArI,451}$ and $n_{N2,C1}/n_{N2,C0}$ ratios show close values of n_e : at pressure of 2.5 mTorr the n_e grows from 2.5×10^9 up to 2.5×10^{10} cm⁻³ when the remote anode current increases from 5 up to 75 A. At most discharge conditions the Langmuir probe gives the n_e about 2-3 times higher than OES gives while the mw hairpin probe shows n_e like OES. The difference appears due to that Langmuir probe measurements are local, at the same time OES measurements are non-local, averaged over whole discharge length. An ionization degree in the RA discharges changes in a range from $\sim 2.5 \times 10^{-5}$ up to $\sim 2.5 \times 10^{-4}$.

Figure 5 shows plasma potential, electron temperature and density as well as the N₂ dissociation degree for the LP arc as functions of argon fraction in Ar-N₂ mixtures. The V_p , T_e and n_e weakly depend on the mixture composition at Ar fraction >20% because ionization potentials of Ar atoms (15.76 eV) and N₂ molecules (15.6 eV) are close. The N₂ dissociation degree increases with Ar fraction. The dependence is opposite to case of the large-area low-pressure glow discharge studied in our paper [10] in which N₂ dissociation degree decreases with Ar fraction. The difference is because of higher, as compared with low-pressure glow discharge, T_e in the low-pressure arc, which amounts about 2-3 eV. Estimations show, provided that T_e and n_e change a little with Ar fraction in the mixture, the Ar_m^* density rises with increase in Ar fraction and the most probable mechanism of N₂ dissociation in the low-pressure arc conditions is excitation transfer from Ar_m^* to N₂:



4. Low-pressure arc modeling

The low pressure arc in large volume was modeled in axially-symmetric drift-diffusion approximation using commercial COMSOL FEM software [14]. The arc discharge is ignited between small cathode mimicking vacuum arc cathode spot and primary arc anode consisting discharge tube walls and chevron baffle installed in front of the cathode, and the primary arc feeds a large area discharge in space between the primary discharge and remote arc anode at the opposite end of the discharge tube. The cathode and remote anode are metal discs with small (2 mm) thickness. To mimic the cathode spot emission, the

diameter of the cathode is chosen 5 mm, while diameter of the remote anode is 20 cm. The electron current density emitted by the cathode (the electron influx current) is input parameter of the model and depends on argon pressure.

The drift-diffusion model is used for modeling the low pressure arc discharge in argon. As a core of the numerical model the transport equations, which can be expressed in the same form for all particle species, have been considered

$$\frac{\partial n_\alpha}{\partial t} + \nabla \cdot \mathbf{\Gamma}_\alpha = R_\alpha, \quad (5)$$

where the coefficient α denotes either electrons (e), ions (i) or excited neutral particles (n), n_α is the number density of the corresponding species, $\mathbf{\Gamma}_\alpha$ is its flux and R_α is the source term.

The excited particle fluxes $\mathbf{\Gamma}_n$ are expressed in the traditional Fick form while the fluxes of the ions $\mathbf{\Gamma}_i$ and electrons $\mathbf{\Gamma}_e$ are expressed in the drift-diffusion form. In the case of magnetized plasma, diffusion coefficients and mobilities of electrons and ions are generally tensors, which can be expressed using the DC mobility μ_{DC} . The DC mobility is obtained by solving the Boltzmann kinetic equation in the two-term approximation in COMSOL Multiphysics using the *Boltzmann equation* interface. The diffusion coefficients are expressed via their mobility. An equation for the electron energy is solved to obtain the electron temperature.

Species that are considered are electrons (e), ground-state argon atoms (Ar), excited argon atoms (Ar*) and argon atomic ions (Ar⁺). The following seven reactions were included in the model.

Table 1. The reactions which were considered in the model. The cross-sections for the electron impact reactions were taken from the Phelps database [15].

No.	Type	Formula	Energy [eV]
R1	elastic	$e + \text{Ar} \rightarrow e + \text{Ar}$	0
R2	excitation	$e + \text{Ar} \rightarrow e + \text{Ar}^*$	11.5
R3	superelastic	$e + \text{Ar}^* \rightarrow e + \text{Ar}$	-11.5
R4	ionization	$e + \text{Ar} \rightarrow e + \text{Ar}^+$	15.8
R5	ionization	$e + \text{Ar}^* \rightarrow e + \text{Ar}^+$	4.24
R6	Penning ionization	$\text{Ar}^* + \text{Ar}^* \rightarrow e + \text{Ar}^+ + \text{Ar}$	-
R7	metastable quenching	$\text{Ar}^* + \text{Ar} \rightarrow 2\text{Ar}$	-

The transport equations are constrained by Neumann-type boundary conditions. At the anodes, the wall boundary condition is imposed, prescribing the normal flux to the boundary based on the thermal movement of electrons and ions. The sticking coefficient for both the Ar⁺ ions and the Ar* excited atoms is set to 1, which corresponds to 100% recombination/de-excitation probability. An important effect for sustaining the DC plasma at the low pressure is the secondary electron emission from the cathode, which is bombarded by ions. Therefore, an additional boundary condition is imposed on the cathode, setting the outward electron flux proportional to the incident ion flux, i.e. $\mathbf{\Gamma}_e^{\text{out}} = \gamma_p \mathbf{\Gamma}_i^{\text{in}}$, where γ_p is the coefficient of secondary emission.

The Poisson equation constrained by Dirichlet-type boundary conditions is used to calculate potential and then electric field strength is calculated. At the cathode, the electric potential is set to zero while at the anode, the electric potential is given by

$$V = V_0 - R_B I_p - C_B R_B \frac{\partial}{\partial t} V, \quad (6)$$

where V_0 is the voltage at the output from the DC power supply, I_p is the plasma current obtained by integrating the current density over the anode, and $R_B = 100\Omega$ is the resistance of the ballast resistor. In addition, the model assumes quite a strong blocking capacitor with the capacity of $C_b = 80\text{nF}$. This capacitor improves the convergence in the ignition phase and does not influence the results as we are only interested in the stationary state.

The whole model is implemented in the COMSOL Multiphysics simulation package [14]. COMSOL uses the finite element method to discretize the equations above and the resulting system of algebraic equations is solved using the MUMPS solver [14]. The computational grid for this model consists of approximately 110,000 elements. It should be stressed that the mesh has to be resolved very finely especially in the region of the cathode fall.

Figure 6 shows density and temperature of electrons as well as plasma potential in low pressure DC arc discharge calculated within the model near primary and remote anodes and measured by Langmuir probe in the principle discharge as functions of argon pressure. One can see that temperature and density of electrons are higher near the primary anode, as compared with those near the remote anode, at argon pressure ≥ 3 mTorr. The electron temperature near the primary anode as well as near the remote anode diminishes when argon pressure grows and, on contrary, the electron density near both anodes lifts with pressure. The phenomena is well known, increase in pressure leads to rise in ionization rate and to maintain discharge becomes enough a lower electron energy/temperature. The dependence of critical plasma parameters of the remote arc discharge on pressure, shown in figure 6, exhibits good qualitative and acceptable quantitative agreement with the experimental findings. As follows from these results, a decrease in the plasma temperature with increasing pressure is accompanied by an increase in the plasma density. At the same time, the plasma potential decreases indicating an increase of the electrical conductivity of the discharge plasma with an increase of the pressure. The comparison of modeling and experimental results shows weak sensitivity of the model to its given approximations, demonstrating the robust behavior of the model.

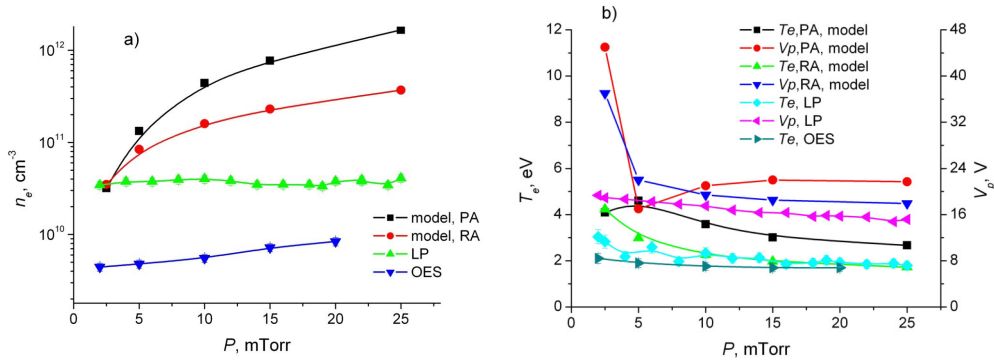


Figure 6. Results of modeling of critical plasma parameters of remote arc discharge as a function of pressure versus experimental findings: (a) n_e , (b) T_e , (c) V_p .

5. Conclusions

The low-pressure arc discharge in large chambers ignited between planar vacuum arc cathode with magnetic steering of arc spots and surrounding grounded primary anode and extended toward remote linear anode was studied. The arc column was moving up and down perpendicular to the cathode-to-remote anode direction, following the movement of the cathodic arc spots. It was found that the arc spot speed increases with increase of the remote arc current and the corresponding increase of the total arc current, resulting in increase of the arc steering magnetic field in agreement with vacuum arc retrograde movement law. The measurements of IEDFs with GEA shows that in RA plasma there are two well-defined groups of ions, one consisting of ions having mean energy of ~several eV and another group with most probable ion energy ~20eV and FWHM ~10-15 eV. The probe measurements show great uniformity the low-pressure arc parameters in the discharge cross sections. T_e and n_e measured with Langmuir probe are a bit higher as compared with the parameters obtained with intensity-ratio methods. It is shown that T_e and n_e in the discharge rely more heavily on pressure and remote anode current and are less dependent on gas composition. N_2 dissociation degree increases with Ar fraction in Ar- N_2 mixtures. The most probable mechanism of N_2 dissociation in the LP arc conditions is excitation transfer between Ar_m^* and N_2 .

Moreover, the low-pressure arc in large volume was modeled in axially symmetric drift-diffusion approximation using commercial COMSOL FEM software. Comparison of calculated and measured dependences of the remote arc critical plasma parameters on argon pressure exhibits good qualitative and acceptable quantitative agreement between measured and calculated values of the parameters: plasma potential, temperature and density of electrons.

References

- [1] Degout D, Farges G, Bergmann E and Dupont D 1993 *Surf. Coat. Technol.* **57** 105.
- [2] Otani K, Sakata N, Ozaki T and Kawabata K 2013 *J. Phys. Conf. Series* **417** 012035.
- [3] Gorokhovskiy V and Del Bel Belluz P 2013 *Surf. Coat. Technol.* **215** 431.
- [4] Böhrk H and Auweter-Kurtz M 2009 *Progress in Propulsion Physics* **1** 381.
- [5] Geva M, Krishnan M and Hirshfield J L 1984 *J. Appl. Phys.* **56** 1398.
- [6] Barengolts S A, Mesyats G A, and Shmelev D L 2001 *J. Experim. and Theor. Phys.* **93**(5) 1065.
- [7] Anders A 2012 *Plasma Sources Sci. Technol.* **21** 035014 .
- [8] Jüttner B 2001 *J. Phys. D: Appl. Phys.* **34** R103.
- [9] *Handbook on Vacuum Arc Science and Technology* 1995 ed. by R Boxman, P Martin and D Sanders (Noes Publications, NJ).
- [10] Avtaeva S, Gorokhovskiy V, Myers S, Robertson S, Shunko E, Zembower Z 2016 *Spectrochimica Acta Part B* **124** 25.
- [11] Stenzel R L 1976 *Rev. Sci. Instrum.* **47** 603.
- [12] Hutchinson I 1987 *Principles of Plasma Diagnostics* (Cambridge University Press, Cambridge).
- [13] Zhu X M and Pu Y K 2010 *J. Phys. D: Appl. Phys.* **43** 403001.
- [14] COMSOL Plasma Module User's Guide. 2012.
- [15] Phelps A V 1999 https://jila.colorado.edu/~avp/collision_data/electronneutral/ELECTRON.TXT